

Supporting information

# Phase transitions in cellulose microfibril dispersions by high energy mechanical de-agglomeration

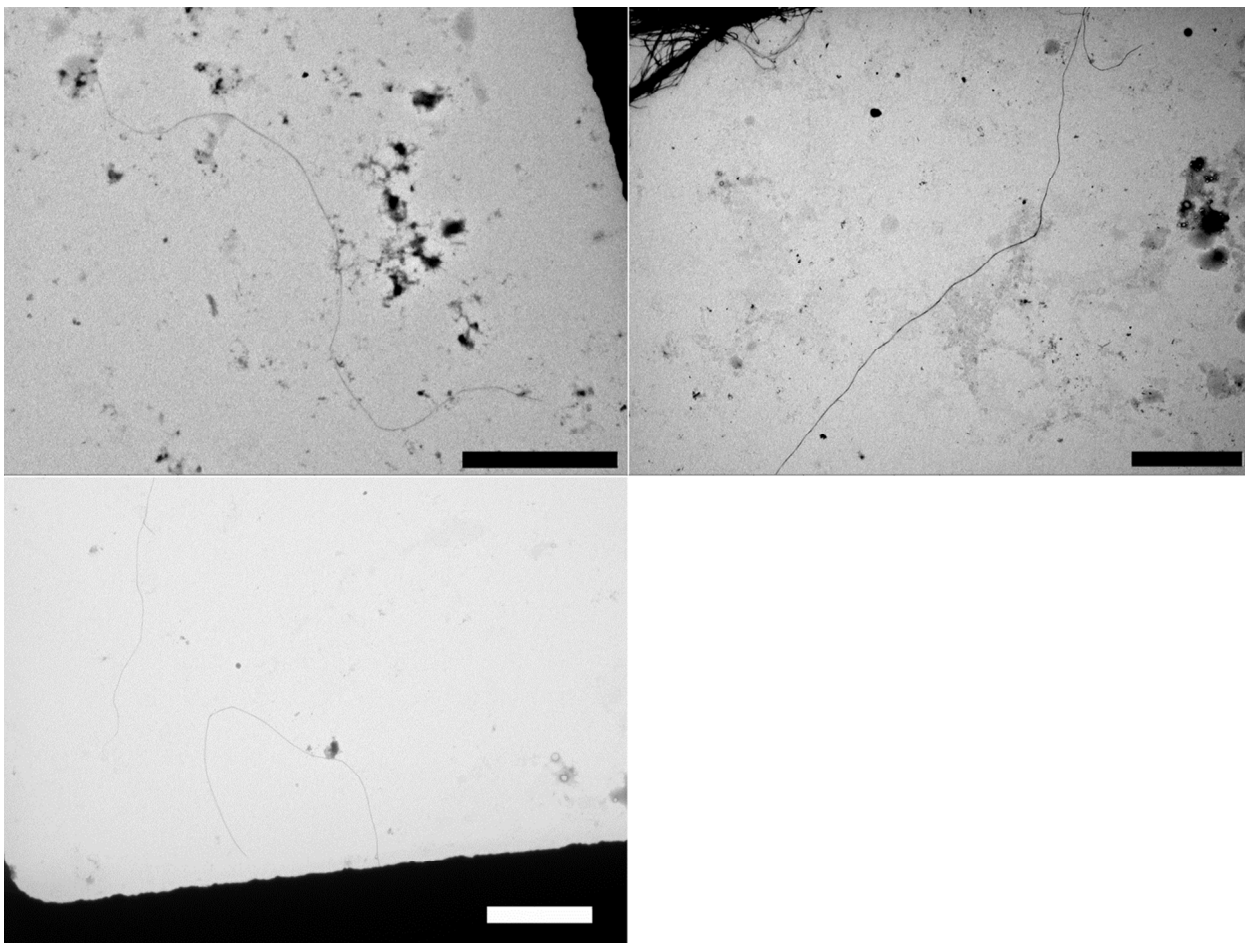
*Sandra J. Veen<sup>†\*</sup>, Anke Kuijk<sup>‡</sup>, Peter Versluis<sup>‡</sup>, Henk Husken<sup>†</sup> and Krassimir P. Velikov<sup>†‡\*</sup>*

<sup>†</sup>Unilever Research Vlaardingen, Olivier van Noortlaan 120, 3133 AT Vlaardingen, The Netherlands

<sup>‡</sup>Soft Condensed Matter, Utrecht University, Princetonplein 1, 3584 CC Utrecht, The Netherlands

### Transmission electron microscopy images of single bacterial cellulose microfibrils

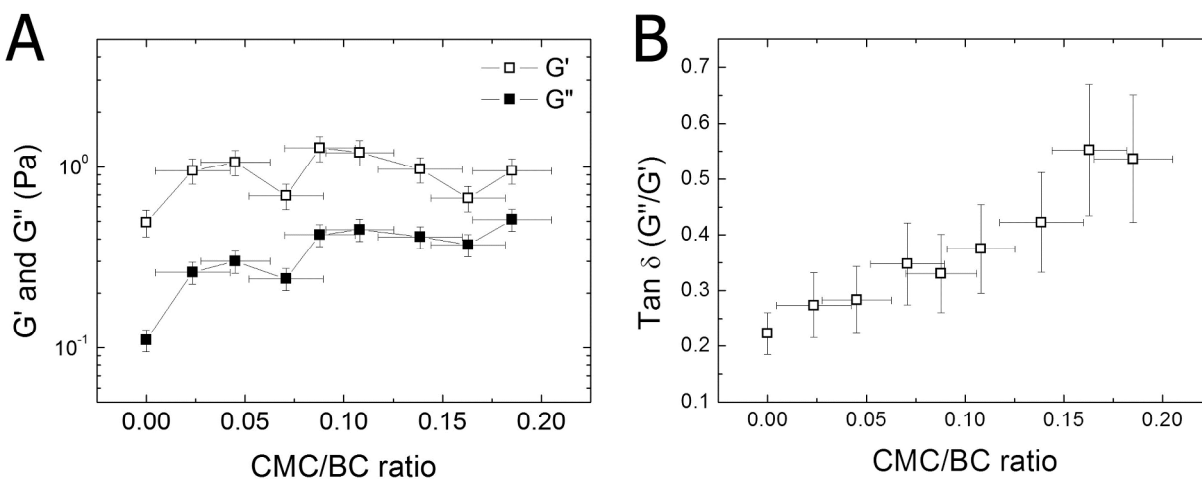
The images were taken from a dispersion of bacterial cellulose (BC) de-agglomerated in the presence of carboxymethyl cellulose (CMC). The weight ratio between CMC and BC was  $\frac{1}{4}$ . The dispersion was de-agglomerated at a BC concentration of 0.8 wt% and diluted to a concentration of  $1 \times 10^{-3}$  wt%. As can be seen in Supporting figure 1, single cellulose microfibrils could be found deposited onto the TEM grid.



**Supporting figure 1.** TEM images of single cellulose microfibrils from a dispersion containing a CMC/BC ratio of  $\frac{1}{4}$ . Scale bars a 5  $\mu\text{m}$ .

## Rheological properties

Rheological measurements were performed on samples containing 0.1 wt% of Bacterial cellulose (BC) and varying ratios of CMC/BC. A stress controlled rheometer (AR G2 or AR 2000, TA Instruments) was used in a plate-plate geometry (plate diameter 4 cm, gap 1 mm). Sand-blasted metal plates were used to prevent slipping. The system was temperature controlled with a Peltier system at a temperature of  $20 \pm 0.1^\circ\text{C}$ . Samples were stirred with a spoon just before placing them in the rheometer. The experimental procedure consisted of 5 minutes of oscillatory shear with a frequency of 1 Hz and 0.1% strain from which both the elastic modulus ( $G'$ ) as well as the loss modulus ( $G''$ ) after 5 minutes were determined. The results are shown in Supporting figure 2.



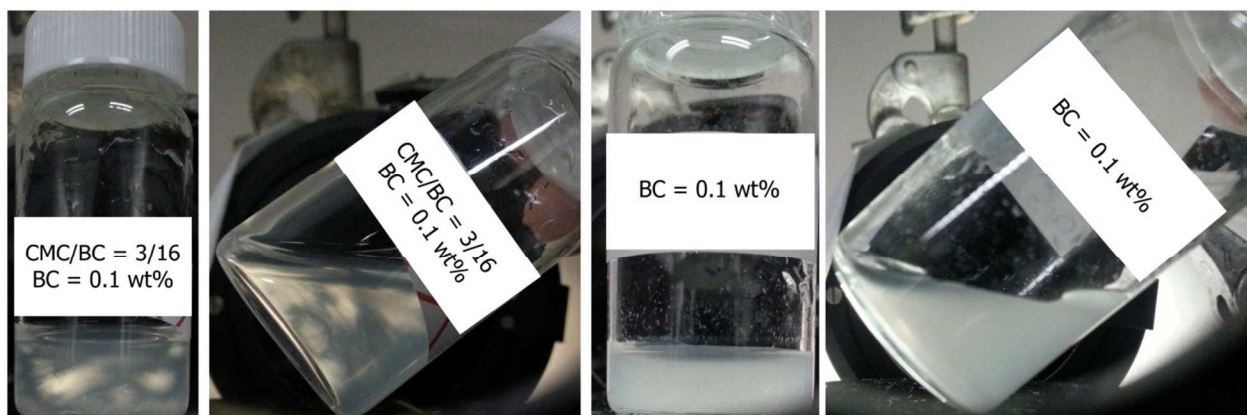
**Supporting figure 2.** (A) Elastic modulus ( $G'$ ), loss modulus ( $G''$ ) and (B) loss tangent of a 0.1 wt% BC suspension with different amounts of CMC added before mechanical treatment.

At a BC concentration of 0.1 wt%, the elastic modulus ( $G'$ ) was higher than the loss modulus ( $G''$ ) for all CMC/BC ratios, indicating gel like behavior (SF 1A). However, as can be seen from the graph above, the loss tangent ( $\tan \delta = G''/G'$ ) does change with increasing CMC content (SF

1B). The system changes to more and more fluid-like behavior as the amount of CMC increases. This is again an indication that the system is more prone to align the fibers since this will lead to less entanglements/contact points and hence a more fluid-like responds. This increased ability of the system to align the fibers was also shown by the appearance of birefringence in the samples with high CMC concentrations.

### Flow of BC dispersions

Light scattering and rheological measurements show that at 0.1 wt% bacterial cellulose al dispersions, regardless of CMC/BC ratio, behave more or less like a gel. However, when sample vials are tilted, all dispersions flow and show more liquid-like behavior. The images below show sample vials containing dispersions of pure BC and of a CMC/BC ratio of 3/16 at 0.1 wt% BC, at rest and tilted at an angle of approximately 45°. Images are taken between crossed polarizers.



**Supporting figure 3.** Images taken between crossed polarizers of BC dispersions at 0.1 wt% for a pure BC dispersion as well as at a CMC/BC ratio of 3/16.

## **Homogeneity from confocal images**

The homogeneity in the cellulose microfibril network was investigated by analyzing the full width half maximum (FWHM) of the normalized intensity distribution of the confocal images. This was done by using the program ImageJ<sup>1</sup>. Images were converted to 8 bit grayscale. Normalization of the intensities was done by using the enhance contrast option of the program with a saturated pixels level of 0.4%. The full width half maximum (FWHM) of the obtained intensity distribution histogram was divided by the number of grayscales which is 256 for 8 bit images. This gives a value between 0 and 1 for the FWHM, for which 1 means a completely homogeneous image. Error bars were obtained by averaging the FWHM over 3 to 5 images of the same sample at the same magnification.

## **Determination of adsorbed CMC**

Viscosity measurements of the continuous phase were performed in order to determine the amount of adsorbed CMC. The continuous phase was obtained by centrifugation of the CMC/BC dispersions. A total of 6 mL of dispersion from each CMC/BC sample was divided over three Eppendorf Safe-lock tubes of 2.0 mL. All samples were centrifuged in a Heraeus Biofuge Primo R for 4:45 hours at a speed of 13000 rpm at a temperature of 20°C. After centrifugation the supernatant was removed. Viscosity measurements of the supernatant were performed on an Anton Paar Physica MCR301 rheometer, using a plate-plate geometry (plate diameter 25 mm, gap 0.1 mm). The zero shear viscosity at 20°C was determined by monitoring the shear viscosity while increasing the shear rate from 100 to  $1 \times 10^5 \text{ s}^{-1}$ .

By measuring the amount of CMC still left free in solution, the amount of adsorbed CMC could be determined by the difference between the free CMC and the CMC added before

mechanical treatment. The free CMC was determined by measuring the viscosity of the continuous phase after removing the BC from the CMC/BC dispersions by centrifugation<sup>2</sup>. Centrifugation of entangled systems is not straightforward since CMC present in solution may be caught in the network while it sediments. However, a difference in CMC concentration within the network and the supernatant would lead to an osmotic pressure difference that would lead to either redistribution of the CMC over the two phases or swelling of the sediment<sup>3</sup>. Since no swelling was observed, the CMC was able to redistribute in which case the concentration of the supernatant was representative of the continuous phase.

The application of high energy mechanical treatment, however, not only affects the BC. It is known that polymers like CMC in solution break-up, resulting in a change in both the zero-shear viscosity as well as the transition to shear-thinning behavior<sup>4,5</sup>. The zero-shear viscosity is smaller at the same concentration. For this reason, using an untreated solution of CMC for determination of the viscosity/concentration calibration curve would lead to an underestimation of the concentration of free CMC. To avoid this, mechanical treatment was applied to a solution of CMC of 0.2 wt%. It was assumed that the CMC in this solution was subjected to the same shear forces during mechanical treatment as the CMC in the CMC/BC mixtures. The resulting solution was used to construct a calibration curve from which the free CMC was determined based on the measured viscosity of the supernatants.

## Counterion condensation limit

According to Manning <sup>6</sup>, the counterion condensation takes place when the bare surface charge density ( $\sigma$ ) exceeds a critical value. For a thin cylinder critical charge density ( $\sigma_{crit}$ ) equals:

$$\sigma_{crit} = \frac{e}{2\pi z l_B a}$$

With  $e$  the unit charge,  $z$  the unsigned valency of the counterions,  $l_B$  the Bjerrum length and  $a$  the radius of the cylinder. This equation holds when  $\kappa a < 1$ , with  $\kappa$  the inverse Debye screening length which is of the order of  $1/40 \text{ nm}^{-1}$  for our system. Furthermore, the valency of the counterions is 1 (Na and H-ions), the radius of our microfibrils is  $\sim 30 \text{ nm}$  and the Bjerrum length for water at room temperature is  $0.7 \text{ nm}$ . Putting these values in the equation above leads to a critical bare surface charge density of  $0.0076 \text{ e/nm}^2$ .

The critical bare charge can also be described in the form of the length of the cylinder per unit surface charge  $b$  which then equals  $l_B \times z$ . In this case, since  $z=1$ , the critical value is reached when this length equals the Bjerrum length which is  $0.7 \text{ nm}$ .

In our case however, the radius and the Debye screening length is of a similar order of magnitude as the radius of the microfibril. Hence the use of the equations for a thick cylinder is more appropriate. In this case:

$$\sigma_{crit} = -\frac{e \ln(\kappa a)}{2\pi z l_B a} [\kappa a K_1(\kappa a) / K_0(\kappa a)]$$

In which  $K_1$  and  $K_0$  are modified Bessel functions of the second kind. Filling in the appropriate numbers,  $\sigma_{\text{crit}}$  now equals  $0.036 \text{ e/nm}^2$ .

As can be seen, in each case the critical values for the bare surface charge are lower than the calculated bare surface charge, even for the lowest amount of added amount of CMC (calculated to be  $0.65 \text{ e/nm}^2$  for the ratio CMC/BC 1/16). This would imply that adding more CMC to the system during de-agglomeration, e.g. increasing the CMC/BC ratio beyond 1/16, would not affect the actual surface charge density because  $\sigma_{\text{crit}}$  is already reached and adding more chargeable groups would not lead to more charge on the surface due to counterion condensation.

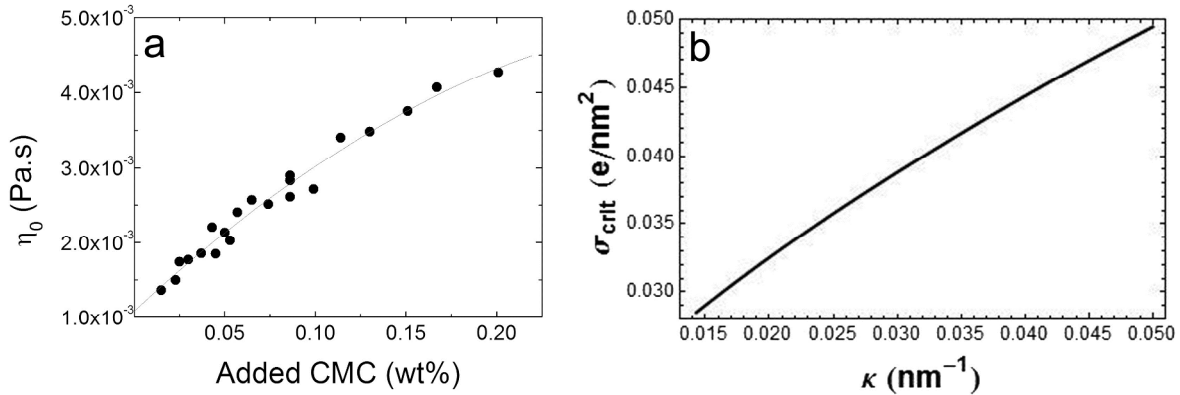
However, we must point out here that the equation for  $\sigma_{\text{crit}}$  for thick cylinders includes the inverse Debye screening length  $\kappa$ . When  $\kappa$  changes, so does  $\sigma_{\text{crit}}$ . In fact,  $\sigma_{\text{crit}}$  increases when more salt is added to the system (leading to a smaller screening length and hence a larger  $\kappa$ ). This effect on  $\sigma_{\text{crit}}$  is shown in the figure below where  $\sigma_{\text{crit}}$  is given as a function of  $\kappa$  over a Debye screening length range from 20 to 70 nm, which are representative values of  $\kappa^{-1}$  for the different suspensions used in this research.

This brings us to the CMC left in the continuous phase, since not all of the CMC molecules adsorb onto the surface of the microfibrils. With increasing CMC/BC ratio, more non-adsorbed CMC remains in the continuous phase (which is evident from viscosity measurements of the continuous phase after centrifugation of the BC, see figure). CMC molecules are elongated molecules in solution due to their stiff and rigid glucose chain backbone<sup>7</sup>. In combination with their small size (as compared to the microfibrils), they can be treated according to Manning's thin rod model. The length of the cylinder per unit surface charge  $b$ , can be estimated from the

degree of substitution (DS=0.8-0.95) and the contour length of the molecule ( $L_c$ ).  $L_c$  is equal to the degree of polymerization (DP=1100) times 0.515 nm (the size of a single glucose unit):

$$b = \frac{L_c}{\text{number of bare charges}} = \frac{DP \times 0.515 \text{ nm}}{DS \times DP} = \frac{0.515 \text{ nm}}{DS} = 0.6 - 0.5 \text{ nm}$$

Since the length of the CMC molecule does not play a role in the final equation, breaking of the CMC molecules due to de-agglomeration (see Supporting information) will not change  $b$ . As you may recall the critical value above which counterion condensation takes place in our system is 0.7 nm. According to the above results, the CMC has not reached this value.



**Supporting figure 4:** (a) Zero-shear viscosity of the supernatant of CMC/BC mixtures after mechanical treatment as a function of the CMC added to the suspension before de-agglomeration. (b) Critical bare surface charge density above which counterion condensation takes place as a function of the inverse Debye screening length for a thick cylinder with a radius of 30 nm in water at room temperature.

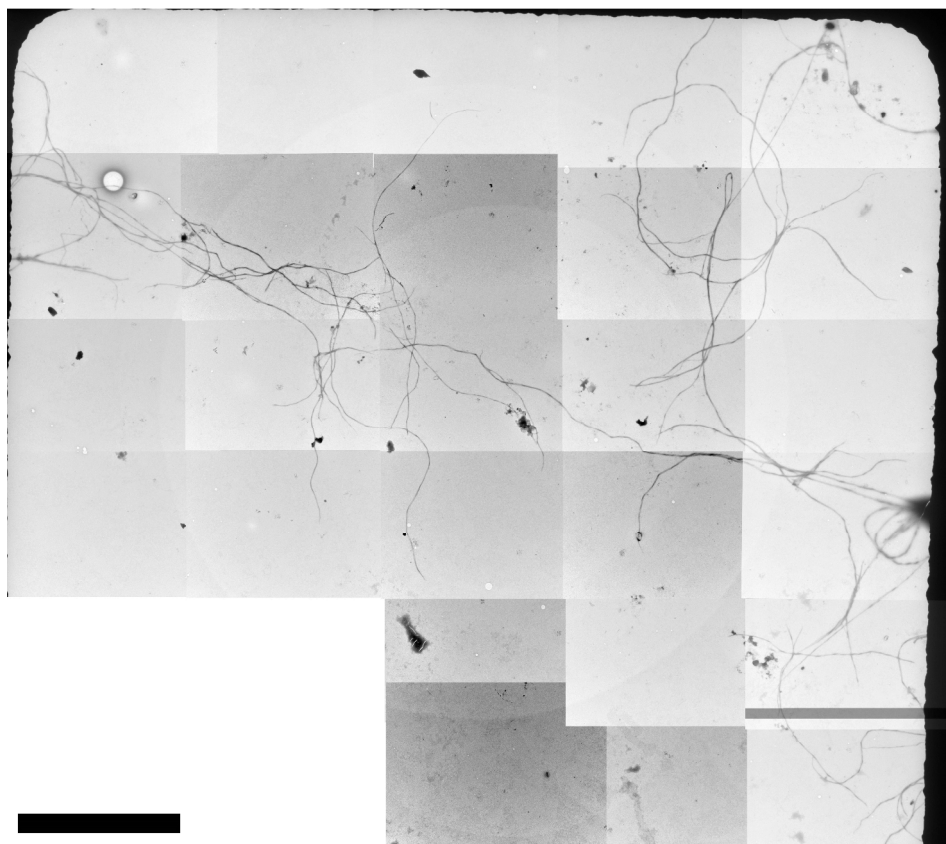
What is more important, as long as the thin rod model applies ( $\kappa a < 1$ ) for the CMC, the surface charge does not depend on the Debye screening length of the system. This means that all the

sodium ions associated with the CMC dissociate and that the counterion concentration is also linearly dependent on the CMC concentration. This increase in salt concentration leads to an increase in inverse Debye screening length and, as argued above, in an increase in the critical bare surface charge density.

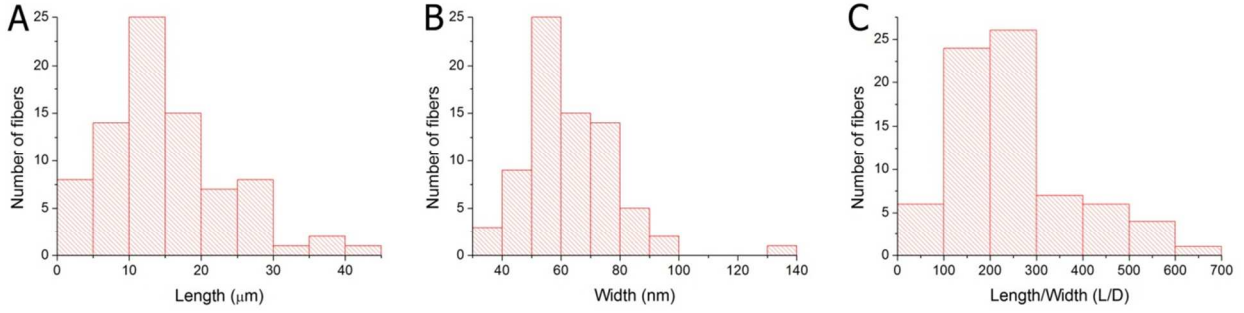
So in short, increasing the CMC/BC ratio during de-agglomeration not only changes the bare surface charge density, but can also increase the critical bare surface charge density or counterion condensation limit.

### **Dimensions and I/N phase transitions of bacterial cellulose fibers.**

From TEM images taken from a dispersion of bacterial cellulose (BC) de-agglomerated in the presence of carboxymethyl cellulose (CMC), large composed images were made from which the length and width distribution could be measured (Supporting figure 4). The weight ratio between CMC and BC was 1/4. The dispersion was de-agglomerated at a BC concentration of 0.8 wt% and diluted to a concentration of  $1 \times 10^{-3}$  wt% and stained with phosphotungsten acid 2 % w/v in water. The resulting distribution in length (L), width (D) and the L/D ratio are given in the histograms in Supporting figure 5.



**Supporting figure 5.** Example of a transmission electron microscopy image used for the measurement of the fiber length and width distribution. Scale bar = 10  $\mu\text{m}$ .



**Supporting figure 5.** Distribution in (A) length, (B) width and (C) length over width ratio for bacterial cellulose fibers.

From the average length and width, theoretical estimates for the isotropic/nematic (I/N) phase transition could be estimated. According to Onsager, the volume fraction ( $\phi$ ) of hard rod particles in the isotropic ( $C_i$ ) and nematic ( $C_n$ ) phase at coexistence are equal to<sup>8,9</sup>:

$$C_i = 3.340 D/L$$

$$C_n = 4.486 D/L$$

Supporting table 1 gives the average values for the measured length, width, D/L ratio and calculated values for the volume fractions of the isotropic and nematic phases. However, since the distribution in size of the fibers is broad, the values are also given for the highest and lowest fiber L/D ratio found for comparison.

In addition, the isotropic and nematic volume fractions are also calculated taking into account the Debye screening length of 40 nm. Adding this to the dimensions of the fiber results in an effective length of  $L+(2\kappa^{-1})$  and an effective diameter of  $D+(2\kappa^{-1})$  and hence affects the value for the I/N phase transition.

**Supporting table 1.** Dimensions of bacterial cellulose fibers, as well as the calculated volume fractions ( $\phi$ ) in the isotropic ( $C_i$ ) and nematic ( $C_n$ ) phases in the phase coexistence regime.

	Length $\mu\text{m}$	Width nm	L/D	D/L	Hard rods		Including Debye length	
					$C_i$ $\phi$	$C_n$ $\phi$	$C_i$ $\phi$	$C_n$ $\phi$
Average	15.11	62	250	$5.48 \times 10^{-3}$	$1.83 \times 10^{-2}$	$2.46 \times 10^{-2}$	$4.27 \times 10^{-2}$	$5.74 \times 10^{-2}$
Maximum	42.45	131	646	$2.18 \times 10^{-2}$	$7.30 \times 10^{-2}$	$9.80 \times 10^{-2}$	$1.70 \times 10^{-1}$	$2.29 \times 10^{-1}$
Minimum	2.61	37	46	$1.55 \times 10^{-3}$	$5.17 \times 10^{-3}$	$6.94 \times 10^{-3}$	$1.30 \times 10^{-2}$	$1.75 \times 10^{-2}$

The experimental transition from isotropic to nematic behavior was seen to occur between 0.04 w% and 0.06 wt% of bacterial cellulose. Taking the density of bacterial cellulose as 1.5 g/mL, the I/N phase transition is then observed to be between  $\phi = 2.6 \times 10^{-4}$  and  $4.0 \times 10^{-4}$ . Compared to the calculated numbers for pure hard rods in Supporting table 1, the observed transition lies two orders of magnitude lower than the calculated one.

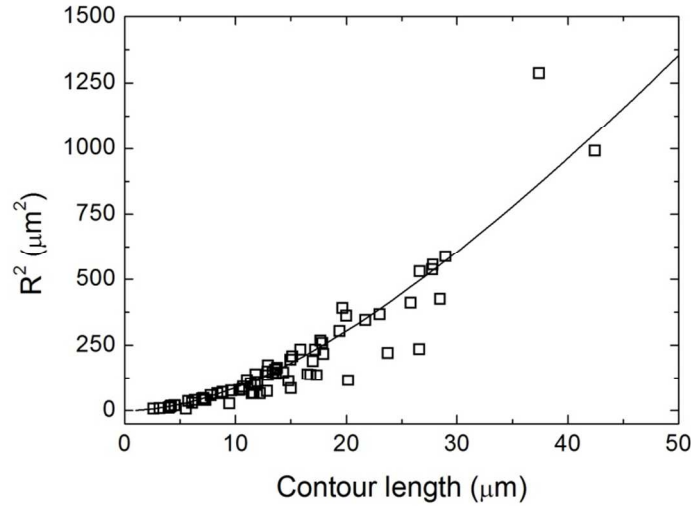
However, taking into account the Debye screening length of  $\sim 40$  nm and the average dimensions of the fibers (9 nm by 60 nm by 15  $\mu\text{m}$ ) an effective volume fraction can be calculated for the experimentally observed transition. The observed I/N transition then lies between  $\phi_{\text{eff}} \sim 6 \times 10^{-3}$  and  $9 \times 10^{-3}$ . This value is much closer to the theoretical value calculated for hard rods including the Debye screening length. In fact, if one compares the theoretical value for the longest fibers found (and hence the lowest D/L ratio), the calculated and observed values are roughly the same order of magnitude.

Considering the shape of the particles in TEM images however, the fibers could more appropriately be considered as semi-flexible. For these particles the theory by Khokhlov-Semenov can be used. However, since our particles are also charged, one also has to take into

account the effective diameter and possible twisting of the particle as was done in the work by Vroege for very long semi-flexible polyelectrolyte<sup>10</sup>. It is now the persistence length instead of the contour length which determines the I/N transition. In order to estimate the persistence length (P) of our particles the following relation between the end-to-end distance (R) of the fibers and their contour length (L) was used as measured in TEM images<sup>11</sup>.

$$\langle R^2 \rangle_{2D} = 4PL \left( 1 - \frac{2P}{L} (1 - e^{-L/2P}) \right)$$

This relation could be fitted to a plot of  $R^2$  as a function of L, yielding a persistence length of  $\sim 11 \mu\text{m}$  (see figure below). Using Vroege's analytical relation for the I/N phase transition for semi-flexible electrolytes this would lead to a volume fraction of  $\sim 7 \times 10^{-2}$  for the theoretical I/N transition. This is of the same order as the transition calculated for rods ( $\sim 1.3 \times 10^{-2}$ ), but slightly higher in volume fraction of what is found for the system ( $\sim 0.9 \times 10^{-2}$ ).



**Supporting figure 6:** Measured squared of the end-to-end distance ( $R^2$ ) versus its contour length of BC fibers as measured by TEM. Black line represents the fit according to Rivettis function for the persistence length.

- (1) Schneider, C. A.; Rasband, W. S.; Eliceiri, K. W. NIH Image to ImageJ: 25 Years of Image Analysis. *Nat. Methods* **2012**, *9*, 671–675.
- (2) Versluis, P.; Popp, A. K.; Velikov, K. P. Interaction between Biopolyelectrolytes and Sparingly Mineral Particles. *Langmuir* **2011**, *27*, 83.
- (3) Faers, M. A.; Choudhury, T. H.; Lau, B.; McAllister, K.; Luckham, P. F. Syneresis and Rheology of Weak Colloidal Particle Gels. *Colloids Surfaces A Physicochem. Eng. Asp.* **2006**, *288*, 170–179.
- (4) Villay, A.; Lakkis de Filippis, F.; Picton, L.; Le Cerf, D.; Vial, C.; Michaud, P. Comparison of Polysaccharide Degradations by Dynamic High-Pressure Homogenization. *Food Hydrocoll.* **2012**, *27*, 278–286.
- (5) Choi, G. N.; Krieger, I. M. Rheological Studies on Sterically Stabilized Model Dispersions of Uniform Colloidal Spheres. *J. Colloid Interf. Sci.* **1986**, *113*, 101–113.
- (6) Manning, G. S. Counterion Condensation on Charged Spheres, Cylinders, and Planes. *J. Phys. Chem. B* **2007**, *111*, 8554–8559.
- (7) Zhivkov, A. M. Electric Properties of Carboxymethyl Cellulose. In *Cellulose - Fundamental aspects*; InTech, 2013.
- (8) Onsager, L. The Effects of Shape on the Interactions of Colloidal Particles. *Ann. New York Acad. Sci.* **1949**, *51*, 627–659.
- (9) Vroege, G. J.; Lekkerkerker, H. N. W. Phase Transitions in Lyotropic Colloidal and Polymer Liquid Crystals. *Rep. Prog. Phys* **1992**, *55*, 1241–1309.
- (10) Vroege, G. J. The Isotropic-Nematic Phase Transition and Other Properties of a Solution of Semi-Flexible Polyelectrolytes. *Polymer (Guildf)*. **1989**, *90*, 4560–4566.
- (11) Rivetti, C.; Guthold, M.; Bustamante, C. Scanning Force Microscopy of DNA Deposited onto Mica: Equilibration versus Kinetic Trapping Studied by Statistical Polymer Chain Analysis. *J. Mol. Biol.* **1996**, *264*, 919–932.